

Order coupling in ferroelectromagnets as simulated by a Monte Carlo method

J.-M. Liu*

*Laboratory of Solid State Microstructures, Nanjing University, Nanjing 210093, China
and International Center for Materials Physics, Chinese Academy of Sciences, Shenyang, China*

Q. C. Li, X. S. Gao, Y. Yang, X. H. Zhou, X. Y. Chen, and Z. G. Liu

Laboratory of Solid State Microstructures, Nanjing University, Nanjing 210093, China

(Received 15 February 2002; revised manuscript received 4 June 2002; published 14 August 2002)

Monte Carlo simulations of the magnetoelectric coupling between ferroelectric order and magnetic order in ferroelectromagnets are performed based on the Janssen model in which the electric and magnetic subsystems are coupled. The simulations reveal that a weak ferromagnetic transition can be activated both by the strong magnetoelectric coupling and by applying external electrical and magnetic fields in either ferroelectric-antiferromagnetic systems or antiferroelectric-antiferromagnetic (AFE-AFM) systems. In addition, a weak ferroelectric order is favored at low temperature in AFE-AFM systems once the magnetoelectric coupling is strong enough. We present in detail our simulated results under various coupling strengths and external fields. A mean-field approach is developed based on the Heisenberg model to explain the simulated phase transitions induced by the coupling. Finally, an experimental relevance of the simulated results is given with our preliminary experiments on the weak ferromagnetic order in $\text{Pb}(\text{Fe}_{0.5}\text{Nb}_{0.5})\text{O}_3$ single crystals.

DOI: 10.1103/PhysRevB.66.054416

PACS number(s): 75.80.+q, 77.80.Bh, 05.10.Ln

I. INTRODUCTION

Ferroelectromagnets (FEM's), i.e., substances where electric order [ferroelectric (FE) or antiferroelectric (AFE)] and magnetic order [ferromagnetic (FM) or antiferromagnetic (AFM)] coexist with their unusual properties, have been attracting scientists for a long time. FEM's were discovered by Russians in the 1950s and subsequently received intensive theoretical and experimental investigations.¹⁻⁵ For this type of material, variation in magnetic parameters and electrical polarization can be observed respectively by applying an external electric field E and a magnetic field H , i.e., the so-called magnetoelectric (ME) effects.^{4,6} These interesting effects enable one to propose different applications in data storage and sensing technologies among many others,⁷ although real applications are still a challenge. The first material exhibiting ME effect is Cr_2O_3 , while most FEM's discovered so far fall into the category of complex perovskite oxides. A perovskite-type structure favors the occurrence of FE or AFE order and typically an AFM order, due to 180° and 90° superexchange in Me-O-Me bonds and strong Jahn-Teller distortion. For an updated bibliography on FEM's and their preparation, crystal structures as well as physical properties refer to the review articles of Venevtsev *et al.*³ and Schmid⁴ and references therein. Furthermore, it was predicted that an extrinsic combination of two crystals with FE (AFE) order and magnetic order, respectively, may generate the ME effect too.⁸

Intensive investigations on ME effects in various FEM's were performed in the past decades. Here, we limit our discussion only to the theoretical (microscopic) aspect. One of the earliest theoretical work can be traced back to 1959 when Landau and Lifshitz predicted the possible existence of the ME effect in some ordered magnetic materials in which an allowed term in the free energy of the form $\alpha_{ij}H_iE_j$, where α_{ij} is the element of a tensor showing the correlation be-

tween H and E .⁹ This phenomenological approach constituted the starting point for the subsequent approaches.^{10,11} Rado proposed his two-ion model to explain the temperature dependence of the ME effect,¹² followed by the improved approaches of Hornreich *et al.*,¹³ Yatom *et al.*,¹⁴ and Gehring.¹⁵ An extensive conceptual and theoretical description of ME effect can be found in the review article of Bonfim *et al.*¹⁶ Without losing the generality, we consider the ME effect induced by applying an electric field. It is now understood that the ME effect originates from symmetry breaking (symmetry lowering) of an AFM crystal or moment canting in an AFM or FM crystal by applying an electric field. There are five mechanisms needed to be considered, i.e., symmetric exchange, dipolar interaction, antisymmetric exchange, single-ion anisotropy, and Zeeman energy.¹⁵ Unfortunately, calculations showed that none of the five mechanisms seems to be dominant for many systems. This makes an exact account of all the five mechanisms very difficult. Furthermore, most of the microscopic theories focus on the effect of an external field. The contribution of intrinsic coupling between the electric and magnetic subsystems to the ME effect has been less emphasized. We name this coupling-induced effect as the magnetoelectric coupling (ME coupling). Such coupling has its origin from at least four mechanisms, i.e., (i) ion displacement or distortion due to the electric dipoles (FE or AFE), which changes the exchange interaction between magnetic ions separating by nonmagnetic ions; (ii) Zeeman splitting due to the exchange-induced internal magnetic field, which affects the electron shell configuration of some magnetic ions and thus the local electric polarization; (iii) Stark effect due to the electric polarization, which changes the spin-orbital and orbital-orbital interactions and thus the magnetic moment; and (iv) coupling between the electric-mechanical interaction and the mechanical-spin one. Experimentally, it was reported that quite a few FEM's show FE-FM coexistence instead of FE

(AFE)-AFM coexistence.¹⁷ It is interesting to know if this difference is due to the ME coupling. In 1994, Janssen developed a model which considers a full combination of electric and magnetic orders.¹⁸ The present authors performed a Monte Carlo (MC) simulation based on the Janssen model in the two-dimensional case and predicted a weak FM transition induced by the coupling in FE-AFM system.¹⁹ Nevertheless, only a preliminary simulation was reported and the problem needed to be addressed.

In this paper, the ME coupling in a mode FEM system is studied by MC simulations. We study the phase transitions in both FE-AFM and AFE-AFM systems. The mean-field approach to this problem will be developed with interesting behaviors to be predicted. In order to establish an at-least qualitative relevance of the simulated results with experiment, single crystals of $\text{Pb}(\text{Fe}_{0.5}\text{Nb}_{0.5})\text{O}_3$ (PFN) were grown and a weak FM transition was confirmed. The paper is organized as follows: we describe the model and the MC algorithm in Sec. II. The simulated results are presented in Sec. III. In Sec. IV, we introduce a mean-field approach to the ME coupling. The experimental relevance and a short summary are given in Secs. V and VI, respectively.

II. MODEL AND PROCEDURE OF SIMULATION

A. Model

The MC simulations are performed for a two-dimensional (2D) squared lattice for which periodic boundary conditions are applied. In order to check whether the presented results can be extended to the three-dimensional case or not, we also perform a sampling in a 3D lattice and compare it with the sampling in the 2D lattice. At each site of the lattice are imposed two order parameters, s_i and u_i , with $s_i = \pm 1$ representing the Ising spin for magnetic interaction and u_i the electrical displacement for the electric interaction. u_i is proportional to the local spontaneous polarization. Therefore there are two subsystems in the lattice, one for magnetic order and the other for electric order. The ME coupling between the two subsystems is taken into consideration. Although this mode lattice was introduced in our earlier work,¹⁹ we repeat it here for readers' convenience. According to the Janssen model,²⁰ the Hamiltonian of the lattice can be written in three parts:

$$\tilde{H} = \tilde{H}^e + \tilde{H}^m + \tilde{H}^{\text{me}}, \quad (1)$$

where \tilde{H}^e represents the Hamiltonian of the electric subsystem, \tilde{H}^m the interaction of the magnetic subsystem, and \tilde{H}^{me} the coupling between the two subsystems.

As approached in the DIFFOUR model,²⁰ the Hamiltonian \tilde{H}^e is given by

$$\tilde{H}^e = \sum_i \left(\frac{p_i^2}{2m} - \frac{a}{2} u_i^2 + \frac{b}{2} u_i^4 \right) - \sum_{\langle i,j \rangle} U_1 u_i u_j - \sum_i E u_i, \quad (2)$$

where $\langle i,j \rangle$ represents a summation over the nearest neighbors, p_i is the momentum at site i , u_i is the electric displacement at site i , a and b are the double-well potential param-

eters, U_1 is the ferroelectric ordering factor, m is the mass and E the electrical field. The three terms in the equation represent the potential energy of site i , the nearest-neighbor electric interaction, and electric static energy, respectively.

\tilde{H}^m in Eq. (1) is the Ising Hamiltonian in which the coupling of the FM-type nearest neighbors and AFM-type coupling of the next-nearest neighbors are taken into account:

$$\tilde{H}^m = - \sum_{\langle i,j \rangle} J_1 \cdot s_i s_j - \sum_{[i,j]} J_2 \cdot s_i s_j - \sum_i H \cdot s_i, \quad (3)$$

where J_1 and J_2 are the FM and AFM couplings factors, respectively, H is the magnetic field, and $[i, j]$ denotes the next-nearest-neighbor pair.

On grounds of the Janssen model, the ME coupling takes the following form:

$$\tilde{H}^{\text{me}} = - \sum_{\langle k,i \rangle, \langle k,j \rangle} \varepsilon_{i,j} \cdot g \cdot u_k^2 \cdot s_i s_j - \sum_{[i,j]} \varepsilon_{i,j} \cdot \kappa \cdot E \cdot s_i s_j, \quad (4)$$

where the first term is the coupling between the two subsystems, g is the coupling factor to scale the coupling strength, the second term is a two-ion term and it takes account of the effect of an electric field on the magnetic spin order as a disturbing term, κ is the electric-field coupling constant. Subscripts i, j in the first term of Eq. (4) denote the nearest neighbors of site k , but i and j refer to different sites. Here we separate the magnetic subsystem into two magnetic sublattices, a and b . Parameter $\varepsilon_{i,j}$ in Eq. (4) is determined by magnetic sublattices to which s_i and s_j belong. $\varepsilon_{i,j} = 1$ if both i and j belong to the first sublattice; and $\varepsilon_{i,j} = -1$ if both belong to the second sublattice, $\varepsilon_{i,j} = 0$ otherwise.

We consider the second order of u_i in Eq. (4) due to the time-reversal and space-reversal symmetries. This property allows us to argue immediately that FE or AFE order has the same contribution to the ME coupling. The FE-AFM and AFE-AFM systems will have similar behaviors in terms of the magnetic response to the coupling. The effect of E on magnetic order is partly ascribed to the second term in Eq. (4). Consequently, the free-energy function is

$$F = - \frac{1}{\beta} \ln \sum_i \exp(-\beta \tilde{H}_i) \quad (5)$$

while the thermodynamic averaging of any physical quantity A is given by

$$\langle A \rangle = \frac{\sum_i A_i \exp(-\beta \tilde{H}_i)}{\sum_i \exp(-\beta \tilde{H}_i)}, \quad (6)$$

where \tilde{H}_i is the i th eigenvalue of Hamiltonian \tilde{H} and A_i the expectation value of A in the i th eigenstate, $\beta = 1/kT$ is the reciprocal of temperature.

Following the derivation given in the earlier work,¹⁹ the magnetic and ferroelectric parameters can then be written as

TABLE I. Parameters selected for the FE-AFM system ($T_N \sim T_E$).

Parameter	a	b	U_1	J_1	J_2	κ
Value	2	20	14	-1	0.2	1

$$m_i = \frac{1}{2L^2} \sum_j^{L \times L} s_j, \quad (7a)$$

$$p_i = \frac{1}{L^2} \sum_j^{L \times L} u_j, \quad (7b)$$

$$S_i = \frac{1}{L^2} \sum_{[i,j]}^{L \times L} \varepsilon_{i,j} \cdot s_i s_j, \quad (7c)$$

where m_i and p_i represent the magnetic moment and electric polarization at any of the MC chain. We therefore obtain the magnetic and ferroelectric parameters:

$$m = \langle m_i \rangle, \quad (8a)$$

$$p = \langle p_i \rangle, \quad (8b)$$

$$\chi_m = \beta (\langle m_i^2 \rangle - \langle m_i \rangle^2), \quad (8c)$$

$$\chi_p = \beta (\langle p^2 \rangle - \langle p \rangle^2), \quad (8d)$$

$$\chi_{me}^1 = \beta (\langle m_i \cdot p_i \rangle - \langle m_i \rangle \langle p_i \rangle), \quad (8e)$$

$$\chi_{me}^2 = \beta (\langle m_i \cdot S_i \rangle - \langle m_i \rangle \langle S_i \rangle), \quad (8f)$$

where m is the magnetization, p the electric polarization, χ_m the magnetic susceptibility, χ_p the polarization susceptibility, and χ_{me} the magnetolectric factor that characterizes the magnitude of the ME coupling. It is separated into two terms: χ_{me}^1 and χ_{me}^2 . They count respectively the contribution of the fluctuation correlation between the spin and electric-dipole order and the two-ion term to the ME effect. In the thermodynamic framework, χ_{me}^1 is quite small. Therefore we treat $\chi_{me}^2 = \chi_{me}$. In our simulation, all of these thermodynamic functions are obtained by statistical averaging the data from the MC configuration chain.

B. Procedure of simulation

The parameters used in our simulations are listed in Tables I and II for FE-AFM and AFE-AFM systems, respectively, where T_N is the Néel point for AFM order and T_E the Curie point for FE order or Néel point for AFE order. The parameters are chosen so that $T_N \sim T_E$ ($T_E > T_N$). The

TABLE II. Parameters selected for the AFE-AFM system ($T_N \sim T_E$).

Parameter	a	b	U_1	U_2	J_1	J_2	κ
Value	2	20	-5	12	-1	0.2	1

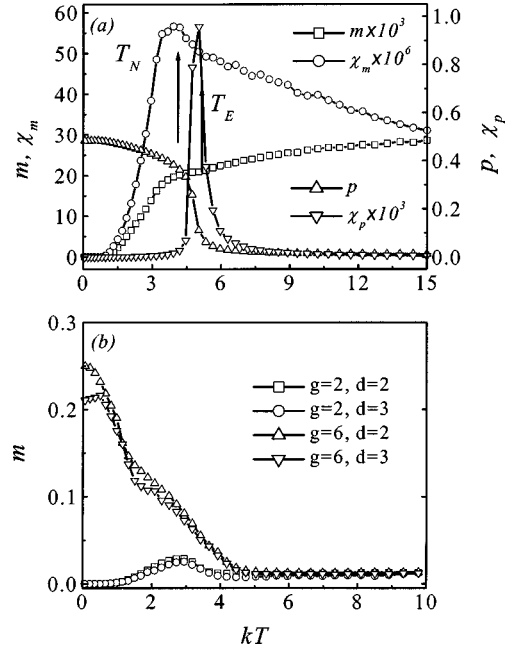


FIG. 1. (a) Simulated magnetization m , electric polarization p , their susceptibilities χ_m and χ_p as a function of kT at $g=0$, (b) the simulated magnetization m as a function of kT in 2D and 3D lattices, respectively. The system is FE-AFM coupled.

sample size for our simulations is $N=L^2$ in the 2D lattice and $N=L^3$ in the 3D lattice, where $L=24$. Variable s_i randomly takes any value within $[-1, 1]$, and u_i is uniformly distributed over $[-0.5, 0.5]$. The MC updating procedure for electric displacement and spin direction at any site is done as follows: at first, the system is initiated as a random lattice, then s_i or u_i is chosen randomly, and the system energy change is calculated. Following the Metropolis algorithm the state (either u_i or s_i) at site i is updated. We repeat this updating for all sites. The simulation is scaled in time with unit of MC step (mcs). One mcs represents one update statistically for each site in the lattice. At each temperature, the first 50 000 mcs are discarded and the thermodynamic averaging are processed during the next 50 000–200 000 mcs.

III. RESULTS AND DISCUSSION

A. FE-AFM system

1. Phase transitions at $g=0$

The phase transitions for the lattice of no ME coupling, i.e., $g=0$ is simulated, as shown in Fig. 1(a) where m and p and their susceptibilities χ_m and χ_p are plotted against kT . For the magnetic subsystem, a typical paramagnetic (PM)-AFM transition around $kT \sim kT_N \sim 3.9$ is observed. The susceptibility χ_m above T_N roughly obeys the Curie-Weiss law $\chi_m = C/(kT - \Delta)$ where C is the Curie constant. As for the electric subsystem, the susceptibility χ_p shows a sharp peak at $kT \sim kT_E \sim 5.0 > kT_N$, indicating a first-order FE transition. Therefore the FE and AFM orders coexist below kT_N .

2. Phase transitions at $g>0$

Before we present the main results for the ME coupling, it is useful to see whether the simulated results in the 2D case

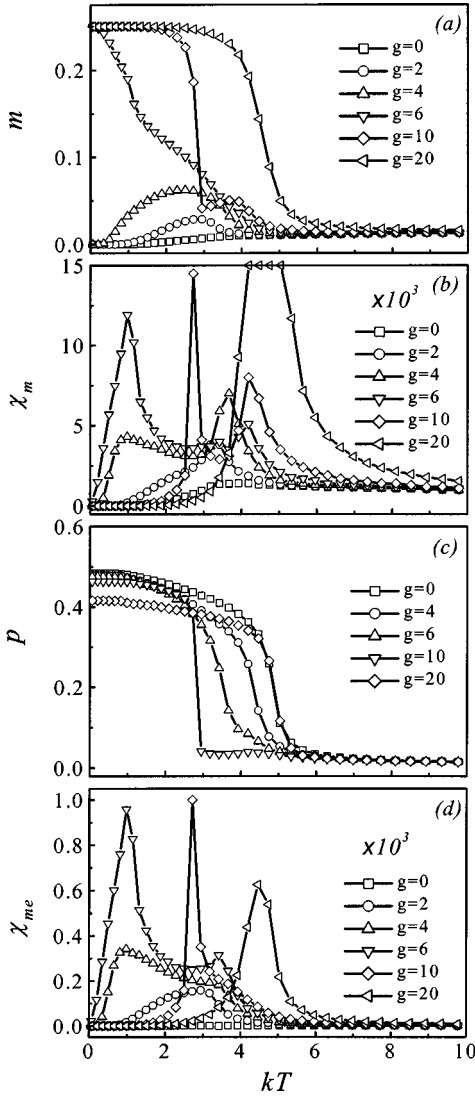


FIG. 2. Simulated magnetization m (a), its susceptibility χ_m (b), electric polarization p (c), and magnetolectric factor χ_{me} (d) as a function of kT at different g in the FE-AFM system.

can be extended to the 3D case or not. An overall 3D simulation seems to be a challenge for us since our computational capability is limited. As an example, the simulated quantity m as a function of kT in the 2D and 3D lattices at two coupling factors, $g=2$ and 6 , is plotted in Fig. 1(b). We leave the details of discussion in sections below, however, it can be found that the results in both lattices are quite similar. The 3D data are slightly smaller than those for the 2D case. This is due to the larger fluctuations in the 3D case than the 2D case. Therefore we are allowed to argue that the simulated results in the 2D lattice can be qualitatively extended to the 3D case. In the sections below, we limit our simulations for the 2D lattice.

Imposing a ME coupling generates the response of m and p as well as of χ_m and χ_p . In Figs. 2(a)–(c) are presented m , χ_m , and p as functions of kT at various coupling factors g . It is demonstrated that a weak FM ordering occurs below a specific kT once the ME coupling is strong enough. At low coupling ($g=0-4$), the magnetization shows a weak peak

over a temperature range ($kT \sim 2.5$), corresponding to a PM-weak FM transition. The peak position shifts to lower kT and its magnitude increases with g . As kT is very low, the AFM order is favored once more. However, when the coupling becomes strong ($g=6$), the AFM order at very low kT is suppressed, and only the FM order is preferred, with m growing with decreasing kT up to a maximum value 0.25 . At $g=10$, a second weak peak (anomaly) appears at $kT=3.5$. This small anomaly disappears as g increases ($g=20$). Such an anomaly can be identified too by the two peaks in the $\chi_m - kT$ curve at $g=10$, which indicates a favored weak FM order even from the PM state as long as the coupling is strong enough.

There is only one peak in the $\chi_m - kT$ curves as g is small ($g=2$), which characterizes the PM-AFM transition. As $g=4$ (and 6), a second peak appears in a lower kT range. The right peak reflects the PM-weak FM transition and the left one is for the weak FM-AFM transition. As $g=20$ and larger, one peak is left that characterizes the PM-FM transition at $T \sim T_E$, while other ordering fluctuations at lower temperature are suppressed completely.

Unlike reported previously,¹⁹ a significant effect of the ME coupling on the FE ordering is identified and the results are shown in Fig. 2(c). At $g=0$, the FE transition occurs at $kT \sim 5.3$, below which the saturated value of p (~ 0.5) is approached with decreasing kT . As g increases from zero to 10 , one observes a remarkable shift of kT_E to low temperature. As $g=10$, the first-order FE transition occurs at $kT \sim 3.0$, the same point as for the appearance of the weak FM order [see Fig. 2(a), $g=10$], after a very weak fluctuation appearing at $kT \sim 4.2$. Note that at this temperature a small anomaly appears for the magnetic subsystem too. Further increasing of g ($=20$ and larger) results in a surprising recovery of the FE transition back to a temperature $T = T_E$ ($g=0$), although the saturated p at low kT is a little lower than 0.5 . This suggests a complete collapse of the AFM order (J_2) in any of the two magnetic sublattices when the ME coupling is extremely strong and virtually no more coupling between the two subsystems exists.

3. Magnetolectric effect

Figure 2(d) shows the ME susceptibility χ_{me} as a function of kT as g takes various values. At $g=0$, χ_{me} is very small, indicating that no remarkable ME effect is activated. A weak peak appears at $kT \sim 2.5$ at $g=2$. As g increases, the second peak appears, and vanishes at $g=20$ and above, leaving only one peak. Therefore the g dependence of the $\chi_{me} - kT$ curve is very similar to that of χ_m . Note that the simulated χ_{me} shows a similar order of magnitude to χ_m and χ_p , confirming the strong-coupling-induced ME effect as revealed in the present system.

From the results presented above, the significant effect of the ME coupling between the electric and magnetic orders on the electric and magnetic properties and thus the ME effect is demonstrated by our simulations.

What should be mentioned here is that the theoretically expected maximum magnetization for the system should be 1.0 instead of 0.25 , supposing the system is in a complete

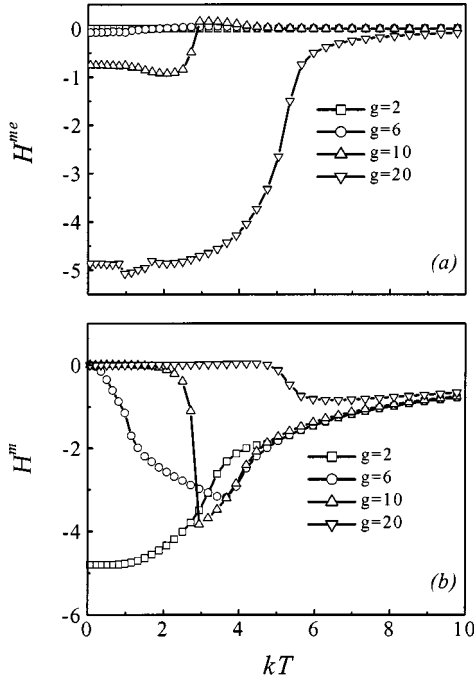


FIG. 3. Hamiltonians \tilde{H}^{me} (a) and \tilde{H}^m (b) at different g in the FE-AFM system.

FM state, because $s_i = \pm 1$ is taken for each site. Therefore the observed FM ordering is a weak FM transition. This weak FM ordering can be explained by a competition between the ME coupling and the AFM interaction, i.e., the competition between \tilde{H}^{me} and \tilde{H}^m . The former causes the inequality of the spin moment in the two sublattices (a and b) and consequently induces a nonzero moment. The latter, however, plays the opposite role since it prefers the AFM order. In Fig. 3 we present the calculated Hamiltonian terms per site for the ME coupling \tilde{H}^{me} and the Ising energy \tilde{H}^m . As g is small ($g=2$), the absolute value of \tilde{H}^m is greater than that of \tilde{H}^{me} , indicating the dominance of AFM order. But when $g=10$, situation reverses since a weak FM order is favored.

To understand the effect of this competition, we discuss the detailed balance condition, which can be written as

$$P_{eq}(x)W(x \rightarrow x') = P_{eq}(x')W(x' \rightarrow x), \quad (9)$$

where

$$P_{eq}(x) = \frac{1}{Z} \exp\left(-\frac{\tilde{H}(x)}{k_B T}\right), \quad (10a)$$

$$\tilde{H}(x) = \tilde{H}^m(x) + \tilde{H}^{\text{me}}(x). \quad (10b)$$

As the coupling is weak, \tilde{H}^{me} can be ignored when compared with \tilde{H}^m . Then the distribution of AFM ordering is favored. When the coupling is strong, \tilde{H}^m can be ignored while compared with \tilde{H}^{me} . So the weak FM ordering is favored.

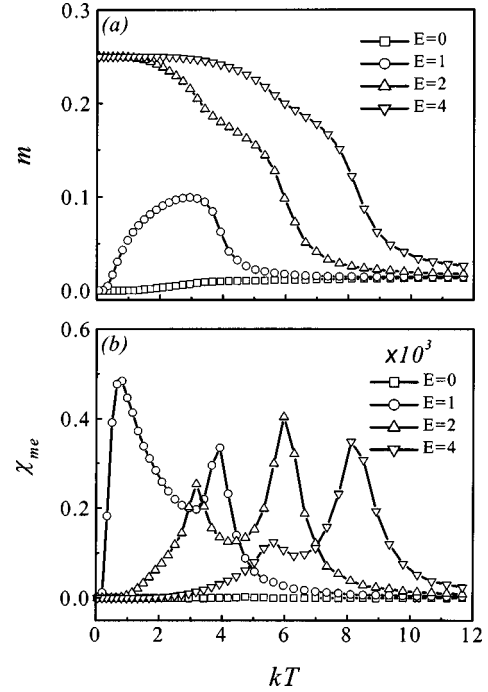


FIG. 4. Simulated magnetization m (a) and magnetoelectric factor χ_{me} (b) as a function of kT under different E at $g=0$ for the FE-AFM system.

4. Effect of external fields

The external field-induced ME effect is also simulated. The results are shown in Fig. 4 ($g=0$) as an example to show the ME effect by applying an electric field. Just looking at the second term on the right side of Eq. (4), the two-ion term, one easily understands that a weak FM order will be favored upon applying a nonzero field E , no matter whether the factor g is zero or not. The weak FM transition point increases with increasing E . A weak second peak in the $\chi_m - kT$ and $\chi_{\text{me}} - kT$ curves, respectively, appears at higher kT , when E is not too large. Further increasing of E suppresses this weak peak (suppressing the AFM order at low kT), leaving the main peak at higher kT . These are quite similar to the effects identified for the case of nonzero coupling. Also note that the field-induced ME effect shows an order of magnitude similar to the case of strong ME coupling, which on the other hand indicates the importance of the ME coupling.

As for the effect of an external magnetic field, one easily understands that applying a magnetic field always favors FM ordering no matter how the ground spin order configuration is, as indicated by the third term of Eq. (3), i.e., the static magnetic energy term.

B. AFE-AFM system

For AFE-AFM systems, we modify the Hamiltonian formulation for the electric subsystem, which reads

$$\begin{aligned} \tilde{H}^e = & \sum_i \left(\frac{p_i^2}{2m} - \frac{a}{2} u_i^2 + \frac{b}{2} u_i^4 \right) - \sum_{\langle i,j \rangle} U_1 u_i u_j \\ & - \sum_{[i,j]} U_2 u_i u_j - \sum_i E u_i \end{aligned} \quad (11)$$

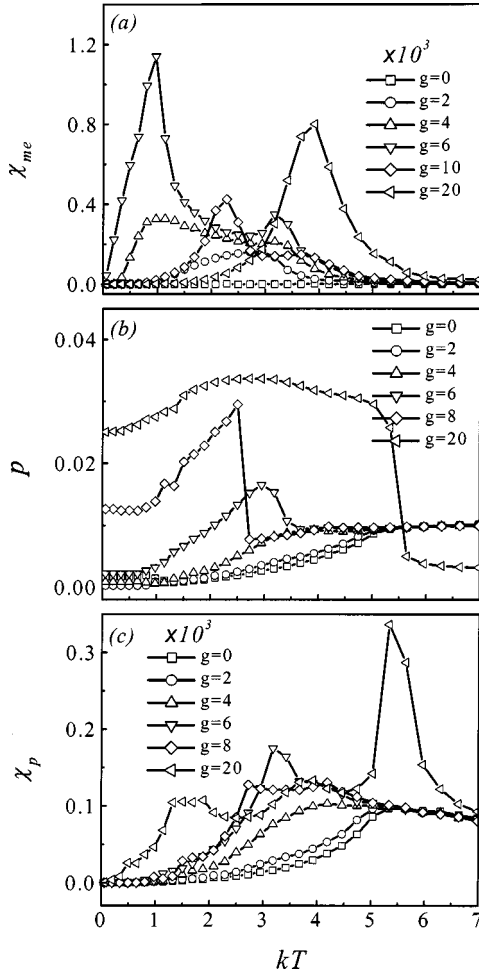


FIG. 5. Simulated magnetoelectric factor χ_{me} (a), electric polarization p and susceptibility χ_p (c) as a function of kT at different g in the AFE-AFM system.

where U_2 represents the AFE ordering factor and counts the next-nearest-neighbor interaction. The other terms remain the same as in Eq. (1). The parameters used in our simulations are listed in Table II. Quite clearly, a weak FM transition can be expected in the AFE-AFM system once the coupling factor g is large enough.

1. Coupling-induced ME effect

We investigate the phase transition behaviors of the two subsystems for various coupling factors g . Parts of the results are presented in Fig. 5. The simulated m - kT , χ_m - kT , and χ_{me} - kT curves are quite similar to those identified for the FE-AFM systems, such as the weak FM ordering with increasing g , appearance of a second peak at medium value of g as well as its disappearance as g is large enough. Figure 5(a) shows the simulated χ_{me} - kT curves as an example. The physics underlying these similarities remains the same too.

An interesting effect as revealed here is the weak FE ordering due to the strong coupling. The simulated p - kT and χ_p - kT curves are shown in Figs. 5(b) and (c). For $g=0$, the simulated kT dependence of p and χ_p shows a clear AFE transition at $kT \sim 5.0$, below which both p and χ_p tend to

zero. This AFE transition is partially suppressed with increasing g and characterized with decreasing of the transition point T_N . However, some fluctuation of the simulated p is already detectable before T decreases down to T_N , as more clearly shown in the χ_p - kT curves. A weak FE order indeed appears for $g \geq 6$ when kT decreases from high value, although the AFE order becomes dominant once more at very low kT . The observed two peaks in the χ_p - kT curves for $g > 6$ mark the paraelectric-FE and FE-AFE transitions, respectively. As g is large enough ($g = 20$), both the AFE order and AFM order are suppressed over the whole temperature range.

While the appearance of the weak FM order can be explained by the ME coupling as formulated by the right first term in Eq. (4), the weak FE order developed with decreasing kT cannot be directly understood, because the FE order and AFE order are degenerate in energy [term u_i^2 in Eq. (4) remains equivalent for the FE and AFE configurations] in the framework of a mean-field approximation, by which it cannot be said that a FE order rather than an AFE order is favored in the present system.

The AFE-FE transition due to the coupling is weak and the obtained polarization p at $g = 20$ is only 0.11 [Fig. 5(b)] instead of the possible maximal value of 0.40 as estimated from the DIFFOUR model [obtained by energy minimization of Eq. (11)]. It means that not all of the lattice sites adopt the FE order. The weak FE and FM orderings due to the coupling can be qualitatively understood by separating the first term of Eq. (4) into two terms. The two terms refer to the two sublattices to which the spin at any site belongs. The first term of Eq. (4) is rewritten as (the second term is neglected here)

$$\bar{H}^{me} = - \sum_{\langle a,i \rangle, \langle a,j \rangle} g \cdot u_a^2 \cdot s_i s_j + \sum_{\langle b,i \rangle, \langle b,j \rangle} g \cdot u_b^2 \cdot s_i s_j, \quad (12)$$

where the subscripts a ($\varepsilon_{i,j} = 1$) and b ($\varepsilon_{i,j} = -1$) refer to the two spin sublattices, respectively. For the favored FM order, the product $s_i s_j$ is positive. From Eq. (12) it is predicted that a large value for u_a and a small value for u_b are favored, which result in a nonzero net electric polarization p over the whole lattice, i.e., a weak FE order. Therefore one may argue that in an AFE-AFM system, the weak FM ordering is the consequence of the ME coupling, and the weak FE ordering is the consequence of the FM ordering. This coupling-induced second-order weak FE order must be weaker than the first-order effect (weak FM order). In fact, as $g = 8-10$, the FM order shows a saturated moment of 0.25 at low kT , while the FE order generates a polarization of only 0.03, much lower than the possible saturated value of 0.11. Unfortunately, the above argument cannot be directly confirmed with the present MC algorithm, since one cannot separate u_i ($i = a$ or b) into two parts referring separately to the two sublattices.

2. Effect of external fields

For the AFE-AFM system ($g = 0$), the effect of E and H on the static properties are simulated too. Similar to the FE-AFM system, the external electric field can induce a weak

FM order. However, applying a magnetic field does not activate any AFE-FE transition. This is expected by looking at Eq. (4) where no term correlating H and u_i is included. What should be mentioned here is that some earlier experiments indeed observed AFE-FE transition activated by applying a magnetic field. This suggests that there are some other interactions not accounted for in the present model should be considered to explain this experimentally identified effect.

IV. MEAN-FIELD APPROACH

A. Mean-field approach

In the last section, we have presented in detail the MC results on the ME effects in both FE-AFM and AFE-AFM systems. In this section, we develop a mean-field approach (MFA) to explain the simulated ME effects. The present MFA starts from the Heisenberg model on the magnetism. The Heisenberg Hamiltonian will be separated into two parts, \tilde{H}^e and $\tilde{H}^m + \tilde{H}^{me}$. Noting the fact that the ME coupling has small effect on the ferroelectric order, especially at small g , i.e., $g=2, 4$, and for the FE-AFM system, we discuss only the second part of the Hamiltonian. Using a standard molecular-field approach available in textbooks of statistical physics, we write the equivalent magnetic field imposing on spin at site i :

$$-\frac{\partial \tilde{H}_m}{\partial s_i} = J_1 \sum_{\langle j \rangle} s_j + J_2 \sum_{[j]} s_j + H, \quad (13)$$

$$-\frac{\partial \tilde{H}_{me}}{\partial s_i} = \varepsilon \cdot g \cdot p^2 \sum_{[j]} s_j + \varepsilon \cdot \kappa \cdot E \sum_{[j]} s_j.$$

The mean-field approximation to Eqs. (13) yields

$$-\frac{\partial \tilde{H}_m}{\partial s_i} = J_1 \cdot z_1 \langle s \rangle + J_2 \cdot z_2 \langle s \rangle + H, \quad (14)$$

$$-\frac{\partial \tilde{H}_{me}}{\partial s_i} = \varepsilon \cdot g \cdot p^2 \cdot z_2 \langle s \rangle + \varepsilon \cdot \kappa \cdot E \cdot z_2 \langle s \rangle,$$

where z_1 and z_2 denote respectively the average number of nearest-neighbor and next-nearest-neighbor ions to site i , $p = \langle u_i \rangle$, with the other parameters defined before.

When Eq. (14) is applied to the two sublattices a and b , we obtain

$$\begin{aligned} -\left(\frac{\partial \tilde{H}_m}{\partial s_i}\right)_a &= J_1 \cdot z_1 \langle s_b \rangle + J_2 \cdot z_2 \langle s_a \rangle + H, \\ -\left(\frac{\partial \tilde{H}_{me}}{\partial s_i}\right)_a &= g \cdot p^2 \cdot z_2 \langle s_a \rangle + \kappa \cdot E \cdot z_2 \langle s_a \rangle, \\ -\left(\frac{\partial \tilde{H}_m}{\partial s_i}\right)_b &= J_1 \cdot z_1 \langle s_a \rangle + J_2 \cdot z_2 \langle s_b \rangle + H, \\ -\left(\frac{\partial \tilde{H}_{me}}{\partial s_i}\right)_b &= -g \cdot p^2 \cdot z_2 \langle s_b \rangle - \kappa \cdot E \cdot z_2 \langle s_b \rangle. \end{aligned} \quad (15)$$

The equivalent magnetic field imposed on the two sublattices are:

$$H_a = H + J_1 \cdot z_1 \langle s_b \rangle + z_2 \cdot [J_2 + (g \cdot p^2 + \kappa \cdot E)] \langle s_a \rangle, \quad (16)$$

$$H_b = H + J_1 \cdot z_1 \langle s_a \rangle + z_2 \cdot [J_2 - (g \cdot p^2 + \kappa \cdot E)] \langle s_b \rangle.$$

The system Hamiltonian is thus written as

$$\tilde{H} = \tilde{H}^m + \tilde{H}^{me} = -H_a \cdot \sum_i s_{ia} - H_b \cdot \sum_i s_{ib}. \quad (17)$$

The average magnetic moment for the two sublattices can be derived from Eqs. (16) and (17):

$$\begin{aligned} m_a &= \frac{\langle s_a \rangle}{2} = \frac{1}{2} \frac{\sum_i s_{ia} \cdot \exp(-\beta \tilde{H}_{ia})}{\sum_i \exp(-\beta \tilde{H}_{ia})} \\ &= \frac{1}{2} \frac{\sum_i s_{ia} \cdot \exp(\beta H_a \cdot s_{ia})}{\sum_i \exp(\beta H_a \cdot s_{ia})} \\ &= \frac{1}{2} \frac{\exp(\beta H_a) - \exp(-\beta H_a)}{\exp(\beta H_a) + \exp(-\beta H_a)} \\ &= \frac{1}{2} th(\beta H_a), \quad s_i = \pm 1 \end{aligned} \quad (18)$$

$$m_b = \frac{\langle s_b \rangle}{2} = \frac{1}{2} \frac{\sum_i s_{ib} \cdot \exp(-\beta \tilde{H}_{ib})}{\sum_i \exp(-\beta \tilde{H}_{ib})} = \frac{1}{2} th(\beta H_b).$$

The system magnetic moment and its susceptibility are

$$m = m_a + m_b, \quad (19)$$

$$\begin{aligned} \chi_m &= \frac{\partial m}{\partial H} = \frac{1}{2} \frac{\partial}{\partial H} (\langle s_a \rangle + \langle s_b \rangle) \\ &= \frac{1}{2} \left[\frac{\partial H_a}{\partial H} \frac{\partial}{\partial H_a} th(\beta H_a) + \frac{\partial H_b}{\partial H} \frac{\partial}{\partial H_b} th(\beta H_b) \right] \\ &= \frac{1}{2} \beta \cdot [\text{sech}^2(\beta H_a) + \text{sech}^2(\beta H_b)]. \end{aligned} \quad (20)$$

The magnetoelectric susceptibility is expressed as

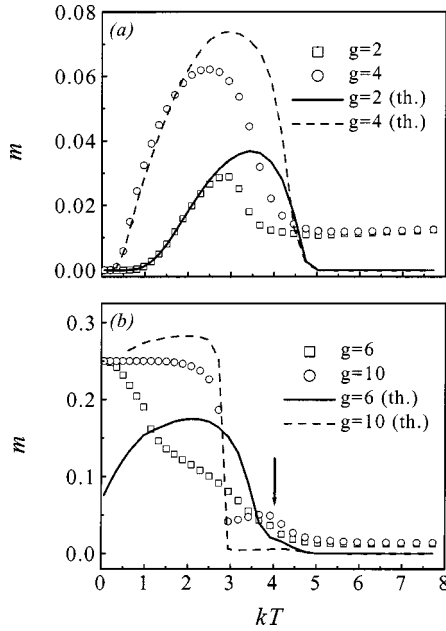


FIG. 6. The simulated (dots) and MFA-calculated (lines) magnetization m as a function of kT at different g in the FE-AFM system. The arrow indicates the second anomaly.

$$\begin{aligned}
 \chi_{\text{me}} &= \frac{\partial m}{\partial E} = \frac{1}{2} \frac{\partial}{\partial E} (\langle s_a \rangle + \langle s_b \rangle) \\
 &= \frac{1}{2} \frac{\partial H_a}{\partial E} \frac{\partial}{\partial H_a} \langle s_a \rangle + \frac{1}{2} \frac{\partial H_b}{\partial E} \frac{\partial}{\partial H_b} \langle s_b \rangle \\
 &= \frac{1}{2} \cdot \kappa \cdot z_2 \cdot \beta [\langle s_a \rangle \text{sech}^2(\beta H_a) - \langle s_b \rangle \text{sech}^2(\beta H_b)],
 \end{aligned} \tag{21}$$

where $th(x)$ and $\text{sech}(x)$ denote the hyperbolic functions. Note that a calculation of m , χ_m , and χ_{me} from Eqs. (19)–(21) requires available values for p_a and p_b . This makes a reliable comparison of the MFA with the simulation impossible, since we found from our simulation that the electric polarization changes as the factor g takes different values.

B. FE-AFM system

We calculate the magnetic and ME properties using the parameters given in Tables I and II. For the FE-AFM system, polarization p at different kT and g takes the simulated data supposing $p_a = p_b$. The temperature dependence of m calculated from the MFA at different g is shown in Fig. 6, where the simulated results are inserted too for comparison. In the qualitative sense, the simulated and calculated magnetization as a function of kT is quite similar. For instance, the MFA predicts the PM-AFM transition as $g=0$. As g increases, a weak FM ordering with decreasing kT before the FM-AFM transition at very low kT is predicted. In particular, the AFM order at very low kT is completely suppressed as g is very large ($g=10$), leaving the weak FM order alone. Note that

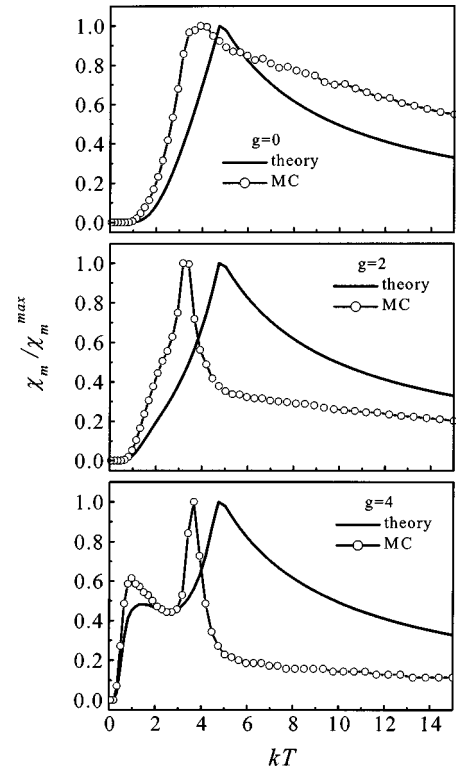


FIG. 7. Comparison between the simulated relative magnetic susceptibility $\chi_m / \chi_m^{\text{max}}$ (MC) and MFA-calculated $\chi_m / \chi_m^{\text{max}}$ (theory) as a function of kT at different g for the FE-AFM system.

the small anomaly around $kT=4.5-3.0$ as $g=10$, as already revealed by the simulations, is also predicted by the MFA calculation (arrow indicated).

However, the difference in the quantitative sense between the simulated and calculated results is substantial. When g is small, the calculated m in the weak FM range is larger than the simulated one, and the calculated FM transition point is higher than the simulated one. As $g=6$, the AFM order is dominant at extremely low temperature from the MFA prediction, but the simulated order is weak-FM type. As regarding the magnetic susceptibility χ_m as a function of temperature, a qualitative similarity between the calculated and simulated results is shown too. However, the calculated χ_m is more than one order of magnitude larger than the simulated values. To illustrate the shape similarity, we present in Fig. 7 the calculated and simulated relative susceptibility $\chi_m / \chi_m^{\text{max}}$ for $g=0, 2$, and 4 as a function of kT . A reasonable agreement in shape between them is achieved although the peak location differs a little from each other. When g is larger, the difference is even more remarkable.

Figure 8 shows the calculated and simulated $\chi_{\text{me}}-kT$ curves at different g . Again, one finds the substantial difference in the order of magnitude between the calculated and simulated results. Nevertheless, when g is small, i.e., $g=2$ and 4 , they are roughly similar in shape. When g becomes even larger ($g=6,10$), one finds the difference is substantial and the MFA seems not work, especially at low temperature.

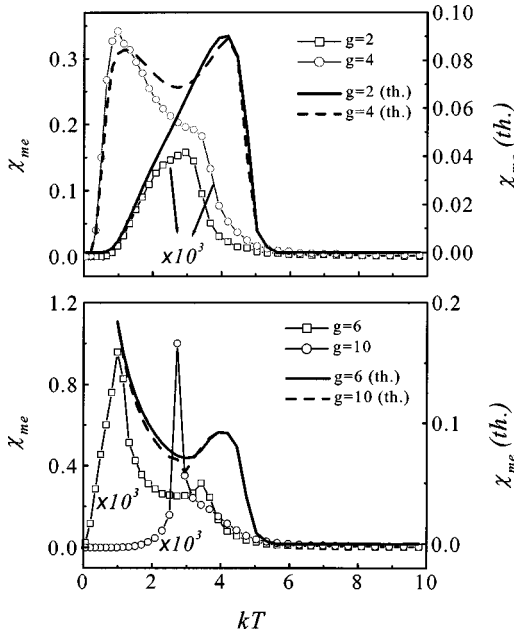


FIG. 8. Simulated magnetoelectric factor χ_{me} (dots+lines) and MFA-calculated χ_{me} [coarse lines, $\chi_{me}(th.)$] as a function of kT at different g for the FE-AFM system.

C. Possible origin of disagreement between MFA and simulation

Basically, the MFA is a quite successful theory on phase transitions far from the critical point. However, a quantitative prediction from the MFA is not always reliable. For the disagreement between the simulated results and the MFA-predicted ones, a satisfactory explanation is not available to us at this moment. The possible reason is that the system stochastic (thermodynamic) fluctuations are not effectively taken into account in the MFA. These fluctuations are suppressed in the MFA by the averaging processing. For example, the two sublattices of the spin configuration may show quite different configuration for u_i due to the ME coupling, which is, however, not considered in the MFA. The MFA simply assumes that the local electric polarization in each lattice site is the same.

One of the consequent effects due to these fluctuations is disordering, while the FM transition and ME coupling are ordering sequences. Because of these disordering fluctuations, the simulated magnetization and susceptibility are smaller than the MFA-predicted values, and the simulated transition point is lower than the calculated point too, as identified in Figs. 6 and 7.

As for the ME coupling, the simulated and calculated χ_{me} are also different from each other in terms of the temperature dependence, especially at low- T range. Since the ME coupling in the FEM's is a second-order effect, it is speculated that the fluctuation-induced suppression may be even larger, which results in much smaller χ_{me} from the simulation than that predicted by the MFA. This effect seems quite significant in the present system.

On the other hand, the polarization p in the MFA is assumed to be an input variable and independent of the coupling factor g . However, for the MFA calculation, the value

of p is taken from the simulated data, which show a dependence on the ME coupling, as shown in Fig. 2(c). We further assumed $p_a = p_b = p$, which is not true in the rigorous sense. Because of the coupling, the real local polarization for sublattices a and b is different from each other. This also contributes to the quantitative failure of the MFA, especially as temperature is low.

D. AFE-AFM system

When the MFA is applied to the AFE-AFM system, no remarkable change in m and χ_m as a function of kT with varying g is obtained, if one takes the simulated system average p as input for the calculation. The failure of the MFA is explained as follows. As suggested from Eq. (16), the system average polarization p in case of AFE order is so small that even large change in g cannot contribute much to H_a and H_b .

We give a more detailed but qualitative discussion below. As stated previously, it is u_i^2 instead of u_i that enters the coupling term in Eq. (4). We divide the electric subsystem into two sublattices c and d and u_i takes positive value in sublattice c (with an average polarization equal to $+p_0$) and negative value in sublattice d (with an average polarization equal to $-p_0$), thus constituting an AFE alignment. The average polarization for the whole lattice may be small ($p = p_0 - p_0 \sim 0$) due to the AFE order, but in each sublattice the polarization is not. We rewrite Eq. (16) as for sublattice c ,

$$H_a = H + J_1 \cdot z_1 \langle s_b \rangle + z_2 \cdot \{J_2 + [g \cdot (+p_0)^2 + \kappa \cdot E]\} \langle s_a \rangle, \quad (22a)$$

$$H_b = H + J_1 \cdot z_1 \langle s_a \rangle + z_2 \cdot \{J_2 - [g \cdot (+p_0)^2 + \kappa \cdot E]\} \langle s_b \rangle,$$

for sublattice d ,

$$H_a = H + J_1 \cdot z_1 \langle s_b \rangle + z_2 \cdot \{J_2 + [g \cdot (-p_0)^2 + \kappa \cdot E]\} \langle s_a \rangle, \quad (22b)$$

$$H_b = H + J_1 \cdot z_1 \langle s_a \rangle + z_2 \cdot \{J_2 - [g \cdot (-p_0)^2 + \kappa \cdot E]\} \langle s_b \rangle,$$

which thus explains qualitatively the simulated weak FM order in the AFE-AFM system.

V. EXPERIMENTAL RELEVANCE

Most FEM's discovered so far, in particular those perovskite oxides, show the FE(AFE)-AFM order at low kT . The AFM Néel point is much higher than the FE Curie point, in many cases. This suggests that the AFM superexchange is very strong in most FEM's.⁴ However, there are quite a few exhibiting the FE-FM (weak) order too.³ Among many other possible mechanisms responsible for the weak FM order, we argue that the ME coupling between the electric and magnetic subsystems is one of the dominant mechanisms. In this section, we report our investigation on the single crystal of PFN, one of those FEM's showing coexistence of FE and

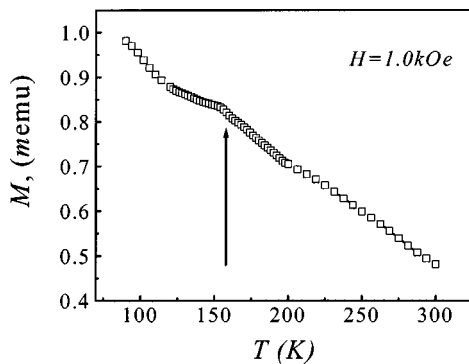


FIG. 9. VSM-measured magnetic moment as a function of T for PFN single crystal. The arrow indicates the anomaly at which a FM ordering is initiated.

weak FM orders under certain temperature although it take FE and AFM orders at very low kT .^{21,22}

PFN has a typical $A(B'B)O_3$ perovskite structure. It is well established that many perovskite niobates are ferroelectrics with quite high T_E . Many iron-based perovskite oxides are strong AFM's due to the strong Fe-O-Fe superexchange, such as $Pb(Fe_{1-x}Ta_x)O_3$, $Pb(Fe_{1-x}W_x)O_3$, etc. The reported T_E for single-crystal PFN is 387 K, for powder PFN it is 143 K. The reported T_N for polycrystalline PFN is ~ 150 K. In our study, the single crystals of PFN are grown from high-temperature solution with PbO as flux with high quality in terms of structure defects and stoichiometry. The high sensitive Mössbauer study on the single crystals was made with the experimental details reported elsewhere.²³ It is confirmed that Fe ions in PFN crystals prefer Fe^{3+} high spin state with no Fe^{4+} identified, similar to earlier reports.^{22,24} The distribution of Fe and Nb ions in the lattice is not quite ordered. The most important fact as revealed by the Mössbauer spectroscopy is that the PM state is favored as $T > 150$ K while the weak FM state is demonstrated as $T < 150$ K. This predicts the possible coupling between the electric order and magnetic order. Here, we present our vibrating sample magnetometer (VSM) data at a very low magnetic field ($H = 1.0$ kOe) in Fig. 9 where the temperature range covered is 80–320 K. With decreasing T , the sample magnetization increases with a clear anomaly at $T = T_m \sim 150$ K, very close to the weak FM transition point as evaluated from the Mössbauer spectroscopy. Below T_m , the magnetization shows no decreasing but further increasing. As T falls down to as low as 80 K, no decaying tendency of the magnetization can be detected. The magnetic hysteresis measured at $T = 90$ K is formed with a ferromagnetic loop, although the remanent polarization is small. Because the

magnetic field for the VSM is so low, one excludes that the magnetization is dominantly field induced, it can be argued that PFN single crystals prefers weak FM order at $T < 150$ K, with no trace of AFM ordering as $T > 80$ K. In fact, the susceptibility measurement presented similar results.²²

The above experiment does establish the relevance between the weak FM order observed in some FEM's, such as PFN, and the coupling between the electric order and magnetic order. From the point of view of practical applications, coexistence of FE and FM orders rather than that of FE and AFM orders in FEM's is preferred. Although we do not yet have direct evidence on the coupling-induced ME effect, the present simulation discloses the essential role of the ME coupling in modulating the ME effect, and thus provides a technical routine for searching for new FEM's with giant ME effect.

VI. CONCLUSION

In conclusion, a Monte Carlo simulation on the magneto-electric effect induced by the ME coupling between electric order (FE and AFE types) and magnetic order (AFM type) in ferromagnetic systems has been performed, based on the Janssen model. It has been revealed that upon the ME coupling strength of the two types of orders, a weak ferromagnetic transition can be activated at low temperature for ferroelectric-antiferromagnetic systems, and both weak ferroelectric and ferromagnetic transitions occur in antiferroelectric-antiferromagnetic systems. We have presented in detail the simulated results on the magnetization and electric polarization as well as their susceptibilities as a function of temperature at different coupling strengths. The magneto-electric susceptibility has been calculated too. In parallel to the simulation, we have also developed a mean-field approach to calculate this coupling induced magneto-electric effect. It has been shown that the mean-field approach can explain qualitatively the simulated phenomena at small coupling strength. Finally, an experimental relevance of the simulation, taking $Pb(Fe_{0.5}Nb_{0.5})O_3$ single crystal as an example, has been presented, which helps us to understand roughly the weak ferromagnetic order in this crystal as temperature is lower than 150 K.

ACKNOWLEDGMENTS

The authors would like to acknowledge the financial support from the Natural Science Foundation of China through the Innovative Group Project and Project No. 50172020, the National Key Program for Basic Research in China (G1998061400-04), and LSSMS of Nanjing University.

*Author to whom all correspondence should be addressed. Email address: liujm@nju.edu.cn

¹G. A. Smolensky, V. A. Isupov, N. N. Krainik, and A. I. Agronovskaya, *Bull. Acad. Sci. USSR, Phys. Ser. (Engl. Transl.)* **25**, 1345 (1961).

²*Magnetolectric Interaction Phenomena in Crystals*, edited by A. J. Freeman and H. Schmid (Gordon and Breach Science Publishers, London, 1975).

³Y. N. Venevtsev and V. V. Gagulin, *Ferroelectrics* **162**, 23 (1994).

⁴H. Schmid, *Ferroelectrics* **161**, 1 (1994).

⁵M. I. Bichurin, *Ferroelectrics* **204**, xvii (1997).

⁶H. Grimmer, *Acta Crystallogr., Sect. A: Found. Crystallogr.* **A48**, 266 (1992).

⁷E. Van Wood and A. E. Austin, *Int. J. Magn.* **5**, 303 (1974).

⁸C. W. Nan, *Phys. Rev. B* **50**, 6082 (1994).

- ⁹L. D. Landau and E. M. Lifshitz, *Electrodynamics of Continuous Media* (Addison-Wesley, Reading, MA, 1960).
- ¹⁰J. F. Scott, Phys. Rev. B **16**, 2329 (1977).
- ¹¹P. Toledano, Ferroelectrics **161**, 257 (1997).
- ¹²G. T. Rado, Phys. Rev. Lett. **6**, 609 (1961); Phys. Rev. **128**, 2546 (1965).
- ¹³R. M. Hornreich and S. Shtrikman, Phys. Rev. **161**, 506 (1967).
- ¹⁴H. Yatom and R. Englman, Phys. Rev. **188**, 793 (1969); **188**, 803 (1969).
- ¹⁵G. A. Gehring, Ferroelectrics **161**, 275 (1994).
- ¹⁶O. F. de Alcantara Bonfim and G. A. Gehring, Adv. Phys. **29**, 731 (1980).
- ¹⁷For example, see A. Maryanowska and J. Pietrzak, Ferroelectrics **162**, 81 (1994).
- ¹⁸T. Janssen, Ferroelectrics **162**, 265 (1994).
- ¹⁹X. S. Gao, J.-M. Liu, X. Y. Chen, and Z. G. Liu, J. Appl. Phys. **88**, 4250 (2000).
- ²⁰T. Janssen and J. A. Tjion, Phys. Rev. B **24**, 2245 (1981).
- ²¹V. A. Bokov, J. E. Myl'nikova, and G. A. Smolenskii, Sov. Phys. JETP **15**, 447 (1962).
- ²²A. Maryanowska and J. Pietrzak, Ferroelectrics **162**, 81 (1994).
- ²³Y. Yang, H. B. Huang, J.-M. Liu, and Z. G. Liu, Ferroelectrics (to be published).
- ²⁴A. Maryanowska and J. Pietrzak, Phys. Status Solidi A **68**, K185 (1981).